Korea-Australia Rheology Journal, 30(1), 1-10 (February 2018) www.springer.com/13367
DOI: 10.1007/s13367-018-0001-2

First-harmonic nonlinearities can predict unseen third-harmonics in medium-amplitude oscillatory shear (MAOS)

Olivia Carey-De La Torre[1] and Randy H. Ewoldt[2,*]

[1]*Department of Mechanical Science and Engineering, University of Illinois at Urbana-Champaign, Urbana 61801, USA*
[2]*Department of Mechanical Science and Engineering and Frederick Seitz Materials Research Laboratory, University of Illinois at Urbana Champaign, Urbana 61801, USA*

(Received August 31, 2017; final revision received November 8, 2017; accepted November 15, 2017)

We use first-harmonic MAOS nonlinearities from G_1' and G_1'' to test a predictive structure-rheology model for a transient polymer network. Using experiments with PVA-Borax (polyvinyl alcohol cross-linked by sodium tetraborate (borax)) at 11 different compositions, the model is calibrated to first-harmonic MAOS data on a torque-controlled rheometer at a fixed frequency, and used to predict third-harmonic MAOS on a displacement controlled rheometer at a different frequency three times larger. The prediction matches experiments for decomposed MAOS measures $[e_3]$ and $[v_3]$ with median disagreement of 13% and 25%, respectively, across all 11 compositions tested. This supports the validity of this model, and demonstrates the value of using all four MAOS signatures to understand and test structure-rheology relations for complex fluids.

Keywords: large-amplitude oscillatory shear, LAOS, MAOS, supramolecular, polymer network, constitutive model testing, prediction, experimental methods, parameter calibration

1. Introduction

Nonlinear large-amplitude oscillatory shear (LAOS) (Ewoldt, 2013; Hyun *et al.*, 2011; Wilhelm, 2002) responses can be written as a power expansion with respect to the input amplitude (Davis and Macosko, 1978; Kirkwood and Plock, 1956; Onogi *et al.*, 1970; Paul, 1969). This power expansion regime has become known as medium-amplitude oscillatory shear (MAOS) (Bharadwaj and Ewoldt, 2015; Ewoldt and Bharadwaj, 2013; Hyun *et al.*, 2007; Hyun and Wilhelm, 2009; Wagner *et al.*, 2011), since it applies to weakly nonlinear signals beyond the linear regime of small-amplitude oscillatory shear (SAOS), but neglects higher order terms that may in general be present in LAOS. The MAOS regime includes two linear (*e.g.* G', G'') and four asymptotically-nonlinear (*e.g.* $[e_1]$, $[e_3]$, $[v_1]$, $[v_3]$) material functions for the shear stress response, which are all a function of frequency ω (Ewoldt and Bharadwaj, 2013). Theoretical calculations in this regime have been reported since the 1950's (Kirkwood and Plock, 1956; Paul, 1969) (for reviews of theoretical work see Bharadwaj and Ewoldt (2015) and Table III in Saengow *et al.* (2017)). Yet, experimental reports sorely lagged, likely due to the experimental challenges of measuring the weakly nonlinear signals of both the first- and third-harmonics of the response.

Perhaps the earliest experimental report of "MAOS" (though this term was not used by the authors) was in 1978 by Davis and Macosko (Davis and Macosko, 1978), who reported first-harmonic MAOS coefficients for polycarbonate and PMMA viscoelastic solids. Third-harmonic MAOS experiments were reported in 2009 by Hyun and Wilhelm (Hyun and Wilhelm, 2009) who considered a single metric related to the amplitude of the third-harmonics. Not until 2013 were experiments published with all four nonlinear coefficients of a MAOS response (Ewoldt and Bharadwaj, 2013), which included decomposed first-harmonic and third-harmonic MAOS measures as a function of frequency for PVA-Borax. MAOS measurements are now more accessible than ever, and being increasingly reported, as the community explores the meaning and value of these material descriptions.

MAOS is the systematic step beyond SAOS, and we invite the reader to study and report MAOS measures for their own materials. MAOS provides more information than SAOS, is amenable to theoretical structure-rheology predictions, and avoids the high dimensionality and potential experimental artifacts of LAOS (Ewoldt, 2013; Ewoldt *et al.*, 2015; Macosko, 1994; Wang *et al.*, 2011; Wilhelm, 2002). One limitation of MAOS is that it only describes the leading order nonlinearities, and therefore may not extrapolate to strong nonlinearities in LAOS, for which local measures along the nonlinear response curve may be beneficial (Ewoldt *et al.*, 2008; Rogers, 2012; 2017). Yet, even in the weakly nonlinear regime beyond SAOS, MAOS is a powerful tool for microstructural inference, model selection, and for fitting nonlinear model

This paper is based on an invited lecture presented by the corresponding author at the 17th International Symposium on Applied Rheology (ISAR), held on May 25, 2017, Seoul.
*Corresponding author; E-mail: ewoldt@illinois.edu

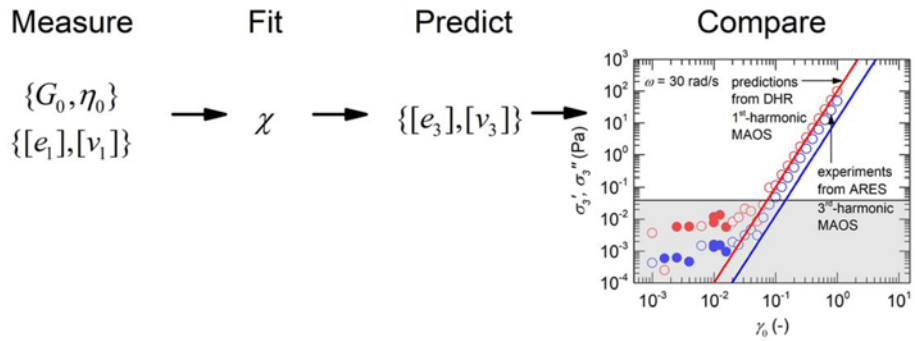

Fig. 1. (Color online) Summary of process to measure first-harmonic rheology, fit model parameters, make predictions of different signals, and compare those predictions to measurements under different conditions.

parameters for physical insight into the material system (Bharadwaj and Ewoldt, 2015; Ewoldt and Bharadwaj, 2013; Gurnon and Wagner, 2012; Hyun and Wilhelm, 2009; Wagner *et al.*, 2011).

In our work here (Fig. 1), we use MAOS to test a structure-rheology model for PVA-Borax (Bharadwaj *et al.*, 2017) by calibrating model parameters to first-harmonic MAOS measures and predicting the otherwise unseen third-harmonic MAOS responses at a different frequency, which we check with additional experiments. PVA-Borax is a well studied material system due to its physical and chemical properties (Chen and Yu, 1997; Inoue and Osaki, 1993; Keita *et al.*, 1995; Kurokawa *et al.*, 1992; Lin *et al.*, 2005; Nemoto *et al.*, 1996). This transient polymer network is an ideal system for studying nonlinear viscoelasticity, as the system shows linear viscoelastic behavior and a single dominant relaxation timescale (Koike *et al.*, 1995) in addition to nonlinear signatures when subjected to large strains (Bharadwaj and Ewoldt, 2015; Ewoldt and Bharadwaj, 2013; Huang *et al.*, 2017). A reversible hydrogel is formed by a di-diol complexation reaction, in which thermoreversible crosslinks form between two diol units of PVA with one borate ion, as shown in Fig. 2.

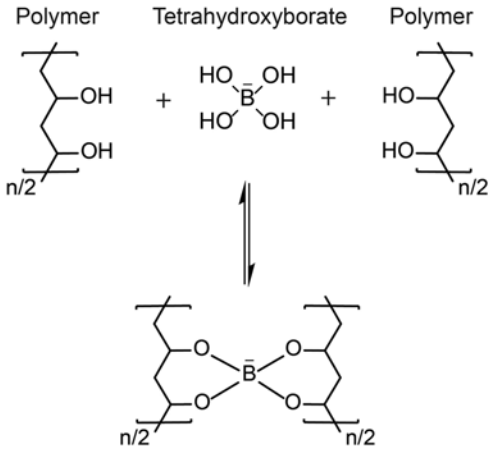

Fig. 2. PVA-Borax crosslink reaction (di-diol). Here, *n* represents the number of monomers in a polymer chain. Four water molecules are omitted from the lower scenario for clarity.

The model of Bharadwaj *et al.* (2017) describes viscoelastic nonlinearities across a range of frequencies, and at present is the only model to correctly predict the signs of the MAOS response for PVA-Borax. The key nonlinear ingredients are embodied in a single nonlinear parameter which we denote as χ, which represents nonlinear stiffening due to both finite extensibility of polymer chains and stretch-induced increase in crosslink density. The model is based on physical insight derived from the signs the four MAOS nonlinearities first reported in Ewoldt and Bharadwaj (2013) (see their Figs. 6 and 7 for interpretations of signs). Our tests of the model will demonstrate the value of first-harmonic MAOS (often overlooked in the recent MAOS literature) and also provide validity of this specific structure-rheology model as it is tested across 11 different compositions of PVA-Borax.

2. MAOS Definitions

A major advantage of oscillatory shear measurements is the decomposition of the stress response into energy storage ("elastic") and energy dissipation ("viscous") responses. For a strain-controlled oscillatory shear measurement, the shear strain input is represented as (Ewoldt, 2013)

$$\gamma(t) = \gamma_0 \sin(\omega t)\,. \tag{1}$$

The shear stress response can be represented by a Fourier series involving higher harmonics,

$$\sigma(t) = \sum_n \sigma_n' \sin(n\omega t) + \sigma_n'' \cos(n\omega t)\,. \tag{2}$$

We will consider a time-periodic response and choose the Chebyshev expansion framework developed by Ewoldt and Bharadwaj (Ewoldt, 2013; Ewoldt and Bharadwaj, 2013) to represent the power expansion of the measurable stress-harmonics because it provides sign interpretations of the four MAOS coefficients (which describe rotation and distortion of Lissajous curves, as shown in Figs. 6 and 7 in

Ewoldt and Bharadwaj (2013)). In this form, the expansion is represented as

$$\sigma_1'(\gamma_0,\omega) = G'(\omega)\gamma_0 + [e_1](\omega)\gamma_0^3 + O(\gamma_0^5) \quad (3)$$

$$\sigma_1''(\gamma_0,\omega) = G''(\omega)\gamma_0 + \omega[v_1](\omega)\gamma_0^3 + O(\gamma_0^5) \quad (4)$$

$$\sigma_3'(\gamma_0,\omega) = -[e_3](\omega)\gamma_0^3 + O(\gamma_0^5) \quad (5)$$

$$\sigma_3''(\gamma_0,\omega) = \omega[v_3](\omega)\gamma_0^3 + O(\gamma_0^5), \quad (6)$$

where $G'(\omega)$ and $G''(\omega)$ are the linear viscoelastic material functions. The four nonlinear MAOS material functions are represented as $[e_1](\omega)$, $[v_1](\omega)$, $[e_3](\omega)$, and $[v_3](\omega)$, where e represents elastic and v represents viscous nonlinearities and the subscripts represent the harmonic of the input frequency. The familiar first-harmonic moduli, and the so-called third-harmonic moduli, are defined by the measurable stresses in Eqs. (3) - (6) normalized by the strain amplitude

$$G_1'(\gamma_0,\omega) = \frac{\sigma_1'}{\gamma_0} = G' + [e_1]\gamma_0^2 + O(\gamma_0^4) \quad (7)$$

$$G_1''(\gamma_0,\omega) = \frac{\sigma_1''}{\gamma_0} = G'' + \omega[v_1]\gamma_0^2 + O(\gamma_0^4) \quad (8)$$

$$G_3'(\gamma_0,\omega) = \frac{\sigma_3'}{\gamma_0} = -[e_3]\gamma_0^2 + O(\gamma_0^4) \quad (9)$$

$$G_3''(\gamma_0,\omega) = \frac{\sigma_3''}{\gamma_0} = \omega[v_3]\gamma_0^2 + O(\gamma_0^4), \quad (10)$$

where G' and G'' appear as plateaus at small strain amplitude, and the dependencies on frequency and amplitude are implied but omitted for clarity (equivalent to that shown in Eqs. (3) - (6)). We will find it useful to use dynamic viscosity, re-framing Eq. (8) as a stress normalized by shear rate amplitude,

$$\eta_1'(\gamma_0,\omega) = \frac{\sigma_1''}{\omega\gamma_0} = \frac{G_1''}{\omega} = \eta' + [v_1]\gamma_0^2 + O(\gamma_0^4). \quad (11)$$

In some recent MAOS literature, there has been a focus on a simplified, single measure Q_0, first defined in Hyun and Wilhelm (2009), which is a normalized magnitude of third-harmonic MAOS (neglecting the third-harmonic phase, and neglecting the first-harmonic MAOS measures). In terms of the variables defined above, this magnitude is calculated as (Hyun *et al.*, 2011)

$$Q_0 = \frac{\sqrt{[e_3]^2 + \omega^2[v_3]^2}}{\sqrt{G'^2 + G''^2}}. \quad (12)$$

We will use all four nonlinear MAOS material functions, rather than a simplified magnitude, since they are explicitly predicted by the model of Bharadwaj *et al.* (2017) and can be reliably measured.

3. Experimental Methods

3.1. Materials and sample preparation

Aqueous solutions of PVA (Aldrich Chemical Co., molecular weight = 85,000–124,000, 99+% hydrolyzed) were mixed with aqueous solutions of sodium tetraborate, *i.e.* Borax (Aldrich Chemical Co.) to form multiple transient polymer networks with thermoreversible transient crosslinks. The mixture was prepared as follows. PVA was dissolved in deionized water under continuous stirring with a magnetic stir rod at a temperature of about 95°C until a homogeneous clear solution was obtained (approximately four hours) to form a 4 wt.% stock solution. Borax was dissolved under similar conditions to form a 4 wt.% stock solution. Throughout the stirring process the containers were sealed with layers of plastic film and aluminum foil to prevent evaporation losses. The solutions were allowed to cool to room temperature under ambient conditions and were mixed together in different ratios to form multiple compositions of a transient polymer network.

The final mixture was prepared by combining measured weights of each component in a closed test tube and stirring them until they were mixed thoroughly. We synthesized eleven different compositions with varying concentrations of both PVA and Borax, as shown in Table 1. Depending on the combination of concentrations of PVA and Borax, it was noticed that the resulting mixture was always a viscous liquid, but sometimes with a high viscosity and noticeable elasticity (*e.g.* material could bounce off of a flat surface when dropped). Higher viscosity samples retaining air bubbles were centrifuged at 3000 rpm for 15 minutes (CL2 Centrifuge, Thermo Scientific) to remove air bubbles before testing.

3.2. Rheological characterization

We use a torque-controlled rotational rheometer and a displacement-controlled rotational rheometer in this work.

Table 1. Summary of the linear parameters $\{G_0, \eta_0, \lambda_0\}$ measured on the stress-controlled rheometer (DHR-3).

Label	Composition (PVA wt.% : Borax wt.%)	G_0 (Pa)	η_0 (Pa·s)	λ_0 (s)
A1	2 : 0.5	94.64	20.78	0.220
A2	2 : 1.25	194.46	42.44	0.218
B1	2.75 : 0.05	148.17	18.99	0.128
B2	2.75 : 0.1	446.66	133.70	0.299
B3	2.75 : 0.5	1013.61	495.97	0.489
B4	2.75 : 1.25	1222.20	511.90	0.419
B5	2.75 : 1.5	1129.29	435.55	0.386
C1	3.5 : 0.05	342.49	50.54	0.148
C2	3.5 : 0.1	999.40	348.40	0.349
C3	3.5 : 0.5	2551.81	1876.68	0.735
C4	3.5 : 1.25	3391.11	2158.69	0.637

It is important to explicitly make a distinction between instruments because we have more confidence in MAOS measurements from a displacement-controlled instrument where torque is measured from a fixed boundary (Merger and Wilhelm, 2014).

Rheological measurements of first-harmonic MAOS measures $[e_1]$ and $[v_1]$ were performed on a stress-controlled combined motor-transducer rotational rheometer (DHR-3, TA Instruments) using a plate-plate geometry (diameter 40 mm, sandblasted) at 25°C maintained by a Peltier system in the lower plate. The loading protocol is outlined as follows. For each test, if the sample had a relatively low viscosity it was poured onto the bottom plate; otherwise, the sample was cut, scooped and placed onto the bottom plate with a spatula. The upper geometry was slowly lowered onto it to prevent stress build-up in the sample. Once the upper geometry was lowered enough to slightly overfill the gap, the sample was trimmed to ensure a proper fill and a solvent trap was used to prevent evaporation losses. Prior to starting any tests, the sample was allowed to relax for 5 minutes to ensure a fully relaxed sample. To characterize the linear viscoelastic (SAOS) regime, strain-sweeps were performed at $\omega = 10$ rad/s starting from $\gamma_0 = 0.01$ until deviations from a linear behavior were observed. We performed a forward and reverse sweep to check for reversibility. A strain amplitude γ_0 was chosen from the linear viscoelastic regime for the SAOS frequency-sweep carried out from $\omega = 0.1$ to $\omega = 100$ rad/s. We identify a storage modulus G_0 and a steady shear viscosity η_0 as plateaus at high and low frequencies, respectively. To characterize the asymptotically nonlinear (MAOS) regime, we analyze the strain-sweeps performed at $\omega = 10$ rad/s, where the MAOS regime is identified by the stress-harmonic nonlinearity exhibiting a scaling of $\sim \gamma_0^3$, as seen in Eqs. (3) - (6). We fit for $[e_1]$ and $[v_1]$ using Eqs. (7) and (8). We perform this protocol for all compositions tested.

Rheological measurements of third-harmonic MAOS measures $[e_3]$ and $[v_3]$ were performed on a strain-controlled separated motor-transducer rotational rheometer (ARES-G2, TA Instruments) using a plate-plate geometry (diameter 50 mm) at 25°C maintained by a Peltier system in the lower plate. The loading protocol was similar to that discussed for measurements on the DHR, except we used mineral oil to prevent evaporation losses. Linear viscoelastic parameters G_0 and η_0 were identified from SAOS frequency-sweeps carried out from $\omega = 0.1$ to $\omega = 100$ rad/s. To characterize the MAOS regime, we identify the scaling of $\sim \gamma_0^3$ from the third-harmonic stress responses and fit for $[e_3]$ and $[v_3]$ using Eqs. (5) and (6). We perform this protocol for all compositions tested.

4. Results

4.1. Linear viscoelastic results

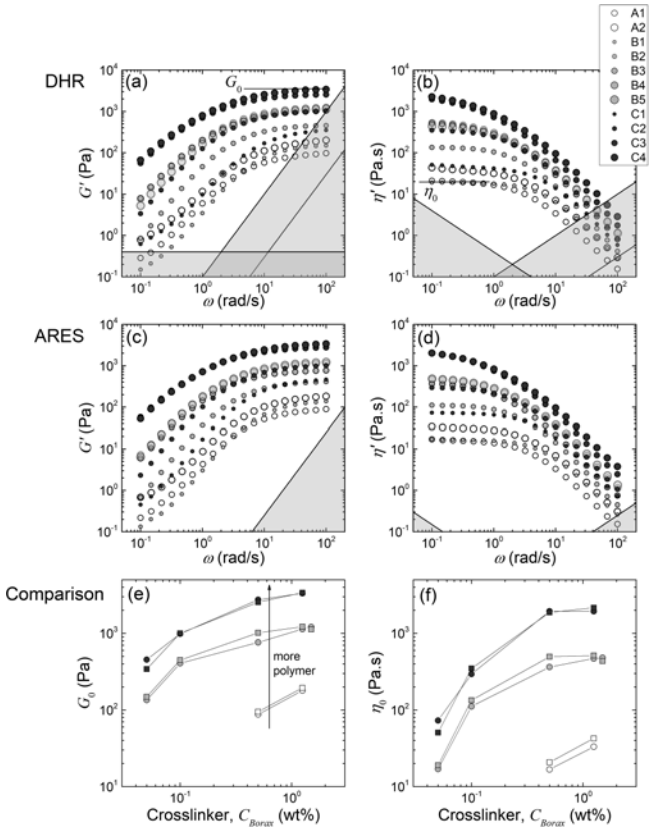

Fig. 3. SAOS frequency-sweep on multiple compositions of PVA-Borax. DHR data are shown in (a) and (b), while ARES data are shown in (c) and (d). The legend shown near (b) is valid for (a)-(d). The linear parameters G_0 and η_0 are compared in (e) and (f), where the squares represent DHR data and circles represent ARES data. The torque limit is shown as a constant line, while the material inertia and instrument inertial limits are shown as lines with scaling $\sim \omega^2$ (Ewoldt *et al.*, 2015).

The linear viscoelastic properties of 11 compositions of PVA-Borax were explored first (Table 1). From the result of the SAOS frequency-sweep for each composition, we fit high and low frequency plateaus to identify the plateau modulus G_0 and the steady shear viscosity η_0, respectively (see Figs. 3a and 3b). A relaxation timescale is defined by the ratio of these linear viscoelastic parameters, $\lambda_0 = \frac{\eta_0}{G_0}$. Table 1 shows the set of linear parameters $\{G_0, \eta_0, \lambda_0\}$ for each composition.

We compare the linear viscoelastic data from the stress-controlled rheometer (DHR) to those from a strain-controlled rheomoeter (ARES) to establish a baseline expectation for agreement between different instruments and different samples. Qualitatively, the data appear to be consistent across the frequency spectrum, as seen in Figs. 3a - 3d. The linear parameters $\{G_0, \eta_0, \lambda_0\}$ are compared in Figs. 3e - 3f and Fig. 4. As expected, the linear parameters qualitatively agree and exhibit the same trends as a func-

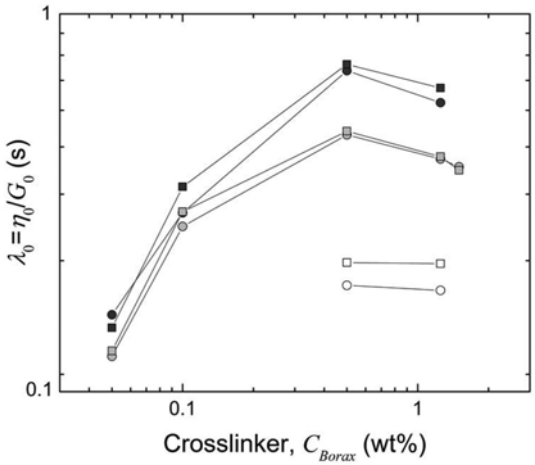

Fig. 4. Comparison between the linear relaxation timescales $\lambda_0 = \frac{\eta_0}{G_0}$ measured from the DHR and ARES from multiple compositions of PVA-Borax. Squares denote DHR data, while circles represent ARES data. Polymer concentration increases with symbol color from white to gray to black.

tion of crosslinker concentration. The linear parameters are expected to agree between instruments since the measurements are made in the linear regime.

In Table 2, we quantify the agreement between instruments using the relative difference between measurements of the linear parameters as a metric. The differences are calculated as

$$\delta_X = \frac{X_{ARES} - X_{DHR}}{X_{ARES}}, \tag{13}$$

Table 2. Summary of the relative difference between measurements of the linear parameters $\{G_0, \eta_0, \lambda_0\}$ from the strain-controlled rheometer (ARES-G2) to those from the stress-controlled rheometer (DHR-3). The differences are calculated using Eq. (13), where $X = \{G_0, \eta_0, \lambda_0\}$ represents the set of linear parameters.

Composition (PVA wt.% : Borax wt.%)	δ_{G_0} (%)	δ_{η_0} (%)	δ_{λ_0} (%)
2 : 0.5	-8.29	-24.23	-14.91
2 : 1.25	-8.65	-27.90	-17.72
2.75 : 0.05	-9.55	-12.18	-3.38
2.75 : 0.1	-9.76	-20.25	-9.33
2.75 : 0.5	-33.22	-36.19	-2.24
2.75 : 1.25	-7.65	-9.12	-1.40
2.75 : 1.5	6.59	9.08	2.08
3.5 : 0.05	24.35	30.51	7.63
3.5 : 0.1	-1.04	-18.36	-17.20
3.5 : 0.5	-7.26	-3.68	-3.92
3.5 : 1.25	-1.65	-11.14	-9.36

where X represents any measured parameter and the subscripts represent which instrument the data were collected on. We observe that the relative difference between measured values of G_0 ranged from approximately 1-30% across all compositions of PVA-Borax. It is worth noting that measurements of G_0 for most compositions had a relative difference less than 10% (with just two exceptions). Similarly, the relative difference between measured values of λ_0 were observed to fall between a relatively small window of approximately 1-15%, in which only three compositions had a relative difference greater than 10%. The relative difference between measured values of η_0 were greater than those of G_0 and λ_0 for almost all compositions (approximately 5-30%, only three compositions less than 10%). On average, measurements of $\{G_0, \eta_0, \lambda_0\}$ differed by {10.7, 18.4, 8.1}% across all compositions, *i.e.* on average having slightly lower values on the ARES instrument (negative values in Table 2).

It is important to note that there appears to be a systematic error between the two instruments since most measurements of $\{G_0, \eta_0, \lambda_0\}$ on the DHR are larger than those measured on the ARES instrument. The disagreement between instruments could come from using different batches of formulated PVA-Borax compositions used for testing on each instrument. Another possible source of error is from instrument calibration, since the disagreement tends to be systematic. Nevertheless, measurements of the linear parameters are reasonably consistent between instruments, as expected. Based on our quantitative observations, it is reasonable to assume that the instruments agree to within 15%. We use this as a baseline expectation for predictions of nonlinear responses between different instruments and different samples.

4.2. Asymptotically nonlinear viscoelastic results

To characterize the asymptotically nonlinear (MAOS) regime, we analyze the strain-sweeps performed at $\omega = 10$ rad/s. The frequency of $\omega = 10$ rad/s was chosen to probe the material near the elastic limit, where $De > 1$ (note $\lambda_{0,\min} = 0.128$ s, Table 1, therefore $De_{\min} = 1.28$). At $\omega = 10$ rad/s, the range of Deborah numbers for all compositions of PVA-Borax were between $De = \lambda_0\omega \approx 1.3$-7, in which it is reasonable to assume that the material behaves more elastically. We could not choose a higher frequency for some compositions because the measurements would be affected by instrument inertia (see Fig. 3). It should be noted that instrument inertia is an artifact of a combined motor-transducer instrument (the DHR in this case). Figure 5 shows the strain-sweeps at 10 rad/s for all compositions tested on the DHR. The MAOS regime is identified by the stress-harmonic nonlinearity exhibiting a scaling $\sim \gamma_0^3$ (Eqs. (3) - (6)), as shown in the right panel of Fig. 5.

We fit for the linear viscoelastic plateaus, G' and η', and the first-harmonic MAOS measures $[e_1]$ and $[v_1]$ at 10 rad/s

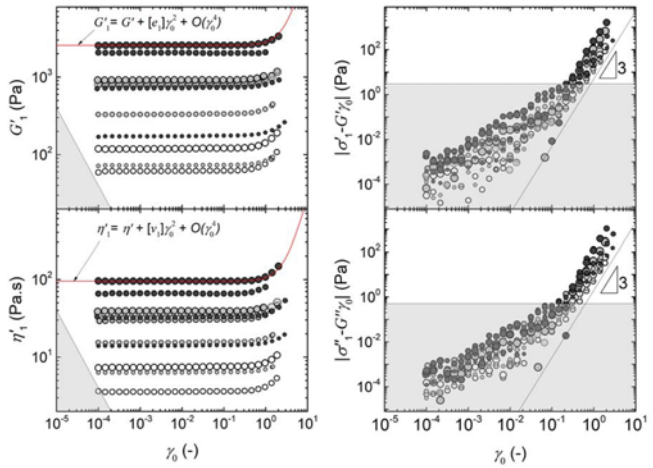

Fig. 5. (Color online) First-harmonic MAOS signatures from strain-sweeps at 10 rad/s on multiple compositions of PVA-Borax performed on DHR. Fit lines from Eqs. (7) and (11). Symbols same as in Fig. 3. Minimum torque noise floor shown in grey. Right panel is transformed stress response data, in which the MAOS regime is identified by a power-law scaling $\sim \gamma_0^3$.

using Eqs. (7) and (8), seen in Fig. 5. It is important to note that there is subjectivity in the process of fitting for material parameters, especially those pertaining to the MAOS regime. There is subjectivity when choosing how many data points to fit since we only want to fit asymptotic changes to the linear baseline. We chose data points up to a 10% change from the linear baseline for our analysis. We followed this procedure for each composition of PVA-Borax tested, and the values for $[e_1]$ and $[v_1]$ are shown in the second and third columns in Table 3.

Table 3. Summary of asymptotically nonlinear parameters measured on the stress-controlled rheometer (DHR). First-harmonic measures $[e_1]$ and $[v_1]$ are used to calculate an estimate of model parameters χ_e and χ_v, respectively. The average $\bar{\chi} = \frac{\chi_e + \chi_v}{2}$ is used as a calibration model parameter to predict third-harmonic MAOS measures.

Composition (PVA wt.% : Borax wt.%)	$[e_1]$ (Pa)	$[v_1]$ (Pa·s)	χ_e (–)	χ_v (–)	$\bar{\chi}$ (–)
2 : 0.5	18.66	0.66	1.34	1.17	1.25
2 : 1.25	26.53	1.39	0.93	1.20	1.06
2.75 : 0.05	12.85	0.81	1.00	0.93	0.96
2.75 : 0.1	72.14	2.63	0.94	1.15	1.05
2.75 : 0.5	172.11	5.99	0.88	1.67	1.27
2.75 : 1.25	126.81	5.29	0.55	1.07	0.81
2.75 : 1.5	119.54	4.37	0.57	0.90	0.74
3.5 : 0.05	26.76	1.31	0.75	0.62	0.68
3.5 : 0.1	83.70	3.5	0.47	0.76	0.61
3.5 : 0.5	16.73	10.47	0.03	1.67	0.85
3.5 : 1.25	258.65	10.44	0.38	1.10	0.74

The values of $[e_1]$ and $[v_1]$ in Table 3 depend on composition. These nonlinear measures generally increase with both polymer and crosslinker concentration (though with a more complicated dependence on crosslinker concentration with some local maxima). Moreover, the trends of $[e_1]$ and $[v_1]$ appear similar, indicating that elastic and viscous nonlinearities are correlated and driven by the same microstructural mechanism. This correlation is consistent with the model of Bharadwaj *et al.* (2017), which predicts that these nonlinearities are exactly correlated. This prediction is based on the physical mechanism of stretch-induced increase in elastic stress (elastic energy), which is concomitant with increased energy dissipation when the stored energy is released by transient crosslink disconnection events. This agreement with the theory, and the correlation of these nonlinearities, is evidence that a single nonlinear parameter can be used to describe the MAOS response for each composition.

4.3. Structure-rheology model and predictions

We use the transient polymer network model of Bharadwaj *et al.* (2017), where the key ingredient for describing a nonlinear response is a single nonlinear parameter, χ. The first-harmonic MAOS measures are related to χ by Eqs. (51) and (53) in Bharadwaj *et al.* (2017),

$$\frac{[e_1]}{G_0} = \frac{5}{6}\chi\left(\frac{De^4\left(De^2+\frac{2}{5}\right)}{(1+De^2)^2(1+4De^2)}\right), \tag{14}$$

$$\frac{[v_1]}{\eta_0} = \frac{3}{4}\chi\left(\frac{De^2\left(De^2+\frac{1}{3}\right)}{(1+De^2)^2(1+4De^2)}\right). \tag{15}$$

In principle, χ could be fit to the full MAOS description which is defined by the four frequency-dependent first- and third-harmonic MAOS measures $\{[e_1](\omega), [v_1](\omega), [e_3](\omega), [v_3](\omega)\}$ defined in Eqs. (7) - (10). Here, we use measurements of the first-harmonic MAOS measures at a single frequency (ω = 10 rad/s) to calibrate χ. Solving for χ in Eqs. (14) and (15) yields an estimate of the model parameter from either the elastic or viscous response, which we denote respevctively as χ_e and χ_v,

$$\chi_e = \frac{6}{5}\frac{[e_1]}{G_0}\left(\frac{(1+De^2)^2(1+4De^2)}{De^4\left(De^2+\frac{2}{5}\right)}\right) \tag{16}$$

and

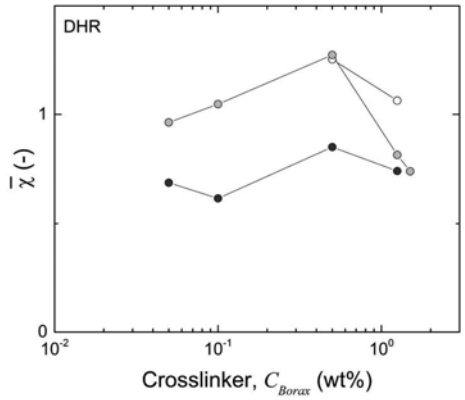

Fig. 6. The parameter $\bar{\chi}$, Eq. (18), calibrated to first-harmonic MAOS parameters $[e_1]$ and $[v_1]$ from the DHR for each PVA-Borax composition tested. Polymer concentration increases with symbol color from white to gray to black.

$$\chi_v = \frac{4}{3}\frac{[v_1]}{\eta_0}\left(\frac{(1+De^2)^2(1+4De^2)}{De^2\left(De^2+\frac{1}{3}\right)}\right). \tag{17}$$

These calculations require calibration of model parameters G_0, η_0 and λ_0 ($De = \lambda_0\omega$), which we take from Table 1. We use the average of χ_e and χ_v

$$\bar{\chi} = \frac{\chi_e + \chi_v}{2} \tag{18}$$

as an estimate of χ for each PVA-Borax composition tested on the DHR. Table 3 shows the values for $\{\chi_e, \chi_v, \bar{\chi}\}$ for each composition and Fig. 6 shows $\bar{\chi}$ as a function of crosslinker.

The third-harmonic MAOS measures are related to χ by Eqs. (52) and (54) in Bharadwaj *et al.* (2017),

$$\frac{[e_3]}{G_0} = \frac{1}{6}\chi\left(\frac{De^4(De^2-2)}{(1+De^2)^2(1+4De^2)}\right), \tag{19}$$

$$\frac{[v_3]}{\eta_0} = -\frac{5}{12}\chi\left(\frac{De^2\left(De^2-\frac{1}{5}\right)}{(1+De^2)^2(1+4De^2)}\right). \tag{20}$$

Thus, we can predict third-harmonic MAOS measures at any frequency by solving for $[e_3]$ and $[v_3]$ in Eqs. (19) and (20) using the linear parameters $\left\{G_0, \eta_0, \lambda_0 = \frac{\eta_0}{G_0}\right\}$ (Table 1) and the calibrated nonlinear model parameter $\bar{\chi}$ (Table 3), where $\chi \to \bar{\chi}$ in Eqs. (19) and (20). Furthermore, we can predict the third-harmonic stress response at any frequency using Eqs. (19) and (20).

Figure 7 is a graphical representation for the process of predicting third-harmonic MAOS from first-harmonic MAOS for 3.5 wt.% PVA with 1.25 wt.% Borax. In sum-

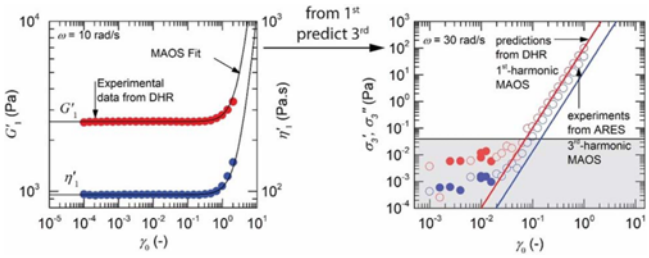

Fig. 7. (Color online) Summary of process for predicting third-harmonic MAOS from first-harmonic MAOS for 3.5 wt.% PVA with 1.25 wt.% Borax. Amplitude sweep data at 10 rad/s (left) is used to obtain first-harmonic MAOS measures $[e_1]$ and $[v_1]$ to predict third-harmonic MAOS measures $[e_3]$ and $[v_3]$ at 30 rad/s, based on the nonlinear transient network model for PVA-Borax from Bharadwaj *et al.* (2017).

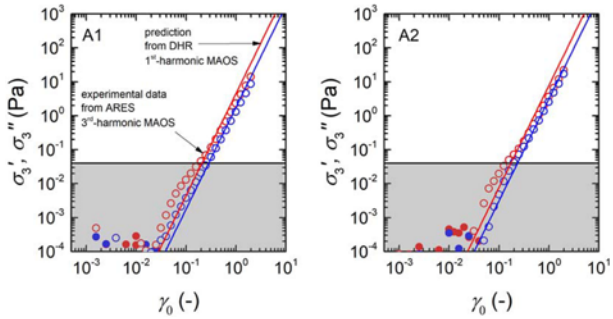

Fig. 8. (Color online) Prediction (lines) versus experiment (symbols) of third harmonic MAOS response at $\omega = 30$ rad/s for compositions of C_{PVA} = 2 wt.% and C_{Borax} = {0.5, 1.25} wt.%. The labels in each graph are the composition labels in Table 1.

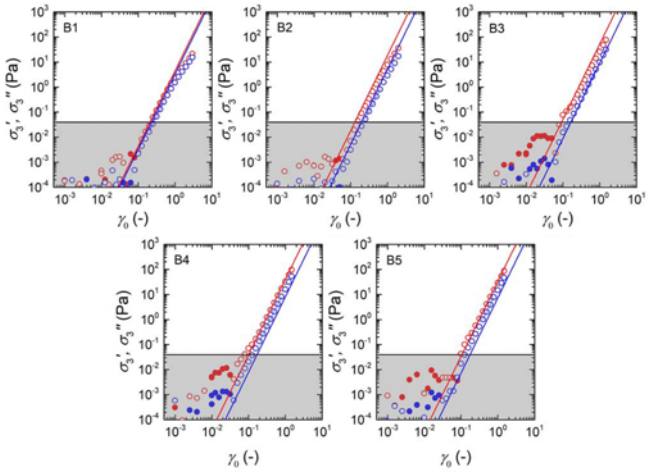

Fig. 9. (Color online) Prediction (lines) versus experiment (symbols) of third harmonic MAOS response at $\omega = 30$ rad/s for compositions of C_{PVA} = 2.75 wt.% and C_{Borax} = {0.05, 0.1, 0.5, 1.25, 1.5} wt.%. The labels in each graph are the composition labels in Table 1.

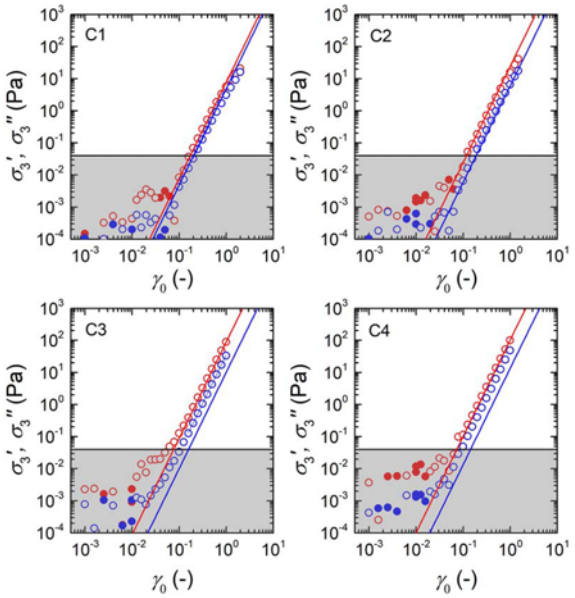

Fig. 10. (Color online) Prediction (lines) versus experiment (symbols) of third harmonic MAOS response at $\omega = 30$ rad/s for compositions of $C_{PVA} = 3.75$ wt.% and $C_{Borax} = \{0.05, 0.1, 0.5, 1.25\}$ wt.%. The labels in each graph are the composition labels in Table 1.

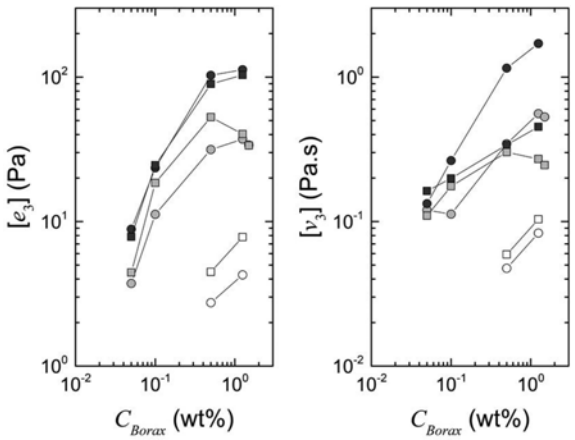

Fig. 11. Comparison of the experimentally observed third-harmonic MAOS parameters from the ARES (circles) and those predicted (squares) from the constitutive model with nonlinear parameter fit to first-harmonic MAOS measurements from the DHR at a different frequency.

mary, we fit $[e_1]$ and $[v_1]$ to strain-sweep data at 10 rad/s from measurements performed on the DHR, calibrate the model parameter $\bar{\chi}$ and predict third-harmonic MAOS measures $[e_3]$ and $[v_3]$ at 30 rad/s, and compare this to measurements on an ARES-G2 rheometer. Third-harmonic data and predictions for all compositions are shown in Figs. 8-10 and Fig. 11 shows a comparison between the observed third-harmonic MAOS parameters (ARES) and the predicted values from first-harmonic MAOS measurements (DHR).

Table 4. Summary of observed and predicted values of $[e_3]$ and $[v_3]$ and their prediction accuracy. Metric is relative difference between fit to third-harmonic data and the prediction value. The differences are calculated using Eq. (21), where $X = \{[e_3], [v_3]\}$.

Composition (PVA wt.% : Borax wt.%)	$[e_3]_{obs}$ (Pa)	$[e_3]_{pred}$ (Pa)	$[v_3]_{obs}$ (Pa·s)	$[v_3]_{pred}$ (Pa·s)	$\delta_{[e_3]}$ (%)	$\delta_{[v_3]}$ (%)
2 : 0.5	2.74	4.48	0.047	0.059	-63.33	-24.58
2 : 1.25	4.27	7.80	0.083	0.104	-82.65	-24.67
2.75 : 0.05	3.73	4.44	0.120	0.110	-18.91	8.47
2.75 : 0.1	11.21	18.48	0.113	0.175	-64.84	-55.87
2.75 : 0.5	31.47	52.74	0.345	0.302	-67.57	12.56
2.75 : 1.25	37.17	40.32	0.558	0.270	-8.48	51.55
2.75 : 1.5	33.85	33.63	0.529	0.246	0.69	53.61
3.5 : 0.05	8.85	7.85	0.133	0.163	11.39	-22.31
3.5 : 0.1	23.48	24.5	0.264	0.199	-4.50	24.65
3.5 : 0.5	102.75	89.53	1.153	0.339	12.87	70.57
3.5 : 1.25	112.42	103.21	1.707	0.453	8.19	73.49

As seen in Figs. 8-10, the agreement between prediction and experimental observation is remarkable, indicating an ability of first-harmonic MAOS to predict otherwise unseen third-harmonic MAOS, even at a frequency three times larger, when a valid constitutive model is available. Table 4 quantitatively summarizes the comparison of observed and predicted values of $[e_3]$ and $[v_3]$, along with relative differences,

$$\delta_X = \frac{X_{obs} - X_{pred}}{X_{obs}}, \tag{21}$$

for each composition of PVA-Borax tested. We use the relative difference as a metric for model prediction accuracy. We observe that the relative difference between values of the third-harmonic elastic parameter $[e_3]$ ranged from approximately 0.5-80% across all compositions of PVA-Borax. Similarly, the relative difference between measured values of the third-harmonic viscous parameter $[v_3]$ were observed to fall between approximately 10-75%. On average, the median magnitude of the relative difference between observed and predicted values of $\{[e_3], [v_3]\}$ is 13% and 25%, respectively, across all compositions.

Although some compositions have larger disagreement, and the model could certainly be improved (*e.g.* with a more complex viscoelastic spectrum rather than a single mode), our general observations agree to within a similar accuracy of the linear viscoelastic parameters tested on different instruments with different batches of sample, as discussed previously with the data in Table 2. Figure 11 graphically compares the predicted and observed values of $[e_3]$ and $[v_3]$ across all compositions. We note that using these decomposed measures for comparison, rather than an overall magnitude (*e.g.* as expressed by Q_0) is a more

rigorous test of this constitutive model.

5. Conclusion

First-harmonic MAOS nonlinearities, taken from the standard and common protocol of strain-amplitude sweep LAOS, are able to predict "unseen" third-harmonic MAOS harmonic data when a valid constitutive model is available. In this case, it is a transient polymer network model (Bharadwaj *et al.*, 2017) applicable to PVA-Borax. Notably, first-harmonic MAOS responses, when fit to the model, were able to correctly predict the signs of the third-harmonic MAOS measures. Furthermore, it is worth noting that no other model predicts the proper signs for the MAOS material functions for PVA-Borax (Bharadwaj *et al.*, 2017). Thus, the transient polymer network is considered a good model for predicting the asymptotically-nonlinear behavior of a PVA-Borax polymer network across the wide range of compositions tested here (with range of G_0 = 100-3000 Pa). The model is better at predicting [e_3] than [v_3] (see Fig. 11). Thus, it can be improved and the disagreement suggests specifically where the model is lacking. We are currently investigating the use of more complex viscoelastic relaxation spectra, and have recently derived the ability to use continuous relaxation spectra with MAOS predictions. This is the subject of a forthcoming publication, which shows improved model fits to frequency-dependent MAOS signatures. For the present work here, which assumed a single relaxation time, the successful predictions are evidence for model validation, and more generally demonstrate the value of first-harmonic MAOS which has often been overlooked in the recent experimental MAOS literature.

Acknowledgements

Research supported by the U.S. Department of Energy, Office of Basic Energy Sciences, Division of Materials Sciences and Engineering under Award No. DE-FG02-07ER46471, through the Frederick Seitz Materials Research Laboratory at the University of Illinois at Urbana-Champaign. For helpful discussions we thank Eric Epstein (MatSE, UIUC), Dr. Luca Martinetti (MechSE, UIUC), and Dr. N. Ashwin Bharadwaj (Nike).

References

Bharadwaj, N.A. and R.H. Ewoldt, 2015, Constitutive model fingerprints in medium-amplitude oscillatory shear, *J. Rheol.* **59**, 557-592.

Bharadwaj, N.A., K.S. Schweizer, and R.H. Ewoldt, 2017, A strain stiffening theory for transient polymer networks under asymptotically nonlinear oscillatory shear, *J. Rheol.* **61**, 643-665.

Chen, C.Y. and T.-L. Yu, 1997, Dynamic light scattering of poly (vinyl alcohol)-borax aqueous solution near overlap concentration, *Polymer* **38**, 2019-2025.

Davis, W.M. and C.W. Macosko, 1978, Nonlinear dynamic mechanical moduli for polycarbonate and PMMA, *J. Rheol.* **22**, 53-71.

Ewoldt, R.H., 2013, Defining nonlinear rheological material functions for oscillatory shear *J. Rheol.* **57**, 177-195.

Ewoldt, R.H., A. Hosoi, and G.H. McKinley, 2008, New measures for characterizing nonlinear viscoelasticity in large amplitude oscillatory shear, *J. Rheol.* **52**, 1427-1458.

Ewoldt, R.H. and N.A. Bharadwaj, 2013, Low-dimensional intrinsic material functions for nonlinear viscoelasticity, *Rheol. Acta* **52**, 201-219.

Ewoldt, R.H., M.T. Johnston, and L.M. Caretta, 2015, Experimental challenges of shear rheology: How to avoid bad data, In: Spagnolie, S.E. eds., *Complex Fluids in Biological Systems*, Springer, New York, 207-241.

Gurnon, A.K. and N.J. Wagner, 2012, Large amplitude oscillatory shear (LAOS) measurements to obtain constitutive equation model parameters: Giesekus model of banding and nonbanding wormlike micelles. *J. Rheol.* **56**, 333-351.

Huang, G., H. Zhang, Y. Liu, H. Chang, H. Zhang, H. Song, D. Xu, and T. Shi, 2017, Strain hardening behavior of poly (vinyl alcohol)/borate hydrogels, *Macromolecules* **50**, 2124-2135.

Hyun, K., E.S. Baik, K.H. Ahn, S.J. Lee, M. Sugimoto, and K. Koyama, 2007, Fourier-transform rheology under medium amplitude oscillatory shear for linear and branched polymer melts, *J. Rheol.* **51**, 1319-1342.

Hyun, K. and M. Wilhelm, 2009, Establishing a new mechanical nonlinear coefficient Q from FT-rheology: First investigation of entangled linear and comb polymer model systems, *Macromolecules* **2**, 411-422.

Hyun, K., M. Wilhelm, C.O. Klein, K.S. Cho, J.G. Nam, K.H. Ahn, S.J. Lee, R.H. Ewoldt, and G.H. McKinley, 2011, A review of nonlinear oscillatory shear tests: Analysis and application of large amplitude oscillatory shear (LAOS), *Prog. Polym. Sci.* **36**, 1697-1753.

Inoue, T. and K. Osaki, 1993, Rheological properties of poly (vinyl alcohol)/sodium borate aqueous solutions, *Rheol. Acta* **32**, 550-555.

Keita, G., A. Ricard, R. Audebert, E. Pezron, and L. Leibler, 1995, The poly (vinyl alcohol)-borate system: Inuence of polyelectrolyte effects on phase diagrams, *Polymer* **36**, 49-54.

Kirkwood, J.G. and R.J. Plock, 1956, Non-Newtonian viscoelastic properties of rod-like macromolecules in solution, *J. Chem. Phys.* **24**, 665-669.

Koike, A., N. Nemoto, T. Inoue, and K. Osaki, 1995, Dynamic light scattering and dynamic viscoelasticity of poly (vinyl alcohol) in aqueous borax solutions. 1. Concentration effect, *Macromolecules* **28**, 2339-2344.

Kurokawa, H., M. Shibayama, T. Ishimaru, S. Nomura, and W.-L. Wu, 1992, Phase behaviour and sol-gel transition of poly (vinyl alcohol)-borate complex in aqueous solution, *Polymer* **33**, 2182-2188.

Lin, H.-L., Y.-F. Liu, T.L. Yu, W.-H. Liu, and S.-P. Rwei, 2005, Light scattering and viscoelasticity study of poly (vinyl alcohol)-borax aqueous solutions and gels, *Polymer* **46**, 5541-5549.

Macosko, C.W., 1994, *Rheology: Principles, Measurements, and Applications*, Wiley-VCH, New York.

Merger, D. and M. Wilhelm, 2014, Intrinsic nonlinearity from LAOStrain-experiments on various strain- and stress-controlled rheometers: A quantitative comparison, *Rheol. Acta* **53**, 621-634.

Nemoto, N., A. Koike, and K. Osaki, 1996, Dynamic light scattering and dynamic viscoelasticity of poly (vinyl alcohol) in aqueous borax solutions. 2. polymer concentration and molecular weight effects, *Macromolecules* **29**, 1445-1451.

Onogi, S., T. Masuda, and T. Matsumoto, 1970, Non-linear behavior of viscoelastic materials. I. Disperse systems of polystyrene solution and carbon black, *J. Rheol.* **14**, 275-294.

Paul, E., 1969, Non-Newtonian viscoelastic properties of rodlike molecules in solution: Comment on a paper by Kirkwood and Plock, *J. Chem. Phys.* **51**, 1271-1272.

Rogers, S.A., 2012, A sequence of physical processes determined and quantified in LAOS: An instantaneous local 2D/3D approach, *J. Rheol.* **56**, 1129-1151.

Rogers, S.A., 2017, In search of physical meaning: Defining transient parameters for nonlinear viscoelasticity, *Rheol. Acta* **56**, 501-525.

Saengow, C., A.J. Giacomin, and C. Kolitawong, 2017, Exact analytical solution for large-amplitude oscillatory shear flow from Oldroyd 8-constant framework: Shear stress, *Phys. Fluids* **29**, 043101.

Wagner, M.H., V.H. Rolón-Garrido, K. Hyun, and M. Wilhelm, 2011, Analysis of medium amplitude oscillatory shear data of entangled linear and model comb polymers, *J. Rheol.* **55**, 495-516.

Wang, S.-Q., S. Ravindranath, and P.E. Boukany, 2011, Homogeneous shear, wall slip, and shear banding of entangled polymeric liquids in simple-shear rheometry: A roadmap of nonlinear rheology, *Macromolecules* **44**, 183-190.

Wilhelm, M., 2002, Fourier-transform rheology, *Macromol. Mater. Eng.* **287**, 83-105.